Evaluating the performance of an Ingot wavefront sensor for the ELT: good news from simulations

Portaluri, Elisa, Viotto, Valentina, Ragazzoni, Roberto, Arcidiacono, Carmelo, Greggio, Davide, et al.

Elisa Portaluri, Valentina Viotto, Roberto Ragazzoni, Carmelo Arcidiacono, Davide Greggio, Kalyan Kumar Radhakrishnan Santhakumari, Maria Bergomi, Simone Di Filippo, Jacopo Farinato, Demetrio Magrin, "Evaluating the performance of an Ingot wavefront sensor for the ELT: good news from simulations," Proc. SPIE 11448, Adaptive Optics Systems VII, 114483I (13 December 2020); doi: 10.1117/12.2562190

SPIE.

Event: SPIE Astronomical Telescopes + Instrumentation, 2020, Online Only

Evaluating the performance of an Ingot wavefront sensor for the ELT: Good news from simulations

Elisa Portaluri[a,b], Valentina Viotto[c,b], Roberto Ragazzoni[d,b,c], Carmelo Arcidiacono[c,b], Davide Greggio[c,b], Kalyan Kumar Radhakrishnan Santhakumari[c,b], Maria Bergomi[c,b], Simone Di Filippo[d,b,c], Farinato Jacopo[c,b], and Magrin Demetrio[c,b]

[a]INAF - Osservatorio Astronomico d'Abruzzo, Via Mentore Maggini, I-64100 Teramo, Italy
[b]ADONI, Laboratorio Nazionale di Ottica Adattiva, Italy
[c]INAF - Osservatorio Astronomico di Padova, Vicolo dell'Osservatorio 5, I-35122 Padova, Italy
[d]Dipartimento di Fisica e Astronomia, Università degli Studi di Padova, Vicolo dell'Osservatorio 3, I-35122 Padova, Italy

ABSTRACT

As the new generation of telescopes is coming soon, we need to solve or improve some issues related to the adaptive optics techniques, necessary to fully exploit the telescopes extraordinary capabilities in terms of sensitivity and resolution. The Ingot wavefront sensor is conceived to overcome some limitations due to the use of artificial sources instead of natural ones: it is designed to cope with the typical elongation of Sodium Laser Guide stars that will be used by the ELTs.

Here we present the preliminary tests we performed to properly set up an end-to-end simulator, in order to evaluate the performance of such a device. We describe the different configurations considered and the assumptions we made, discussing also some computational problems we faced building up the tool. We also show the results of the first simulations obtained closing the loop with a mock ELT telescope.

Keywords: Adaptive Optics, Wavefront Sensing, Ingot WFS, Numerical Simulations, LGS, Sodium Laser Guide Star, ELT

1. INTRODUCTION

The Ingot wavefront sensors (I-WFS) represent a new class of sensors designed to overcome some limitations affecting the adaptive optics (AO) facilities that foresee the use of laser guide stars (LGS) as references for the wavefront correction.[1] "A new fashion for an old paradigm" was the description of such a device, which started with a 6-faces configuration[2] and then reached the final simpler shape,[3] as in Figure 1. The 3-faces ingot prism splits the Na-LGS into three pupils, two of which are reflected off from the top roof and the third pupil reaches the detector without touching the ingot prism.

It is intended to be used by the next generation of extremely large telescopes (i.e. the European Extremely Large Telescope,[4] ELT, and the Giant Magellan Telescope[5]) MCAO modules, which are going to be fed by artificial sources, made by exciting the Sodium layer at around 90 km from the ground with a launcher located at the side of the telescope. As it is commonly known, these sources show some differences from natural stars, first of all being not point-like objects, but something similar to "cigars" in the sky because they are generated at a finite distance and on a layer that has a certain thickness.

To evaluate the impact of this innovative WFS, compared with a classical Shack-Hartmann WFS, we set up an end-to-end simulation tool, carrying out some tests and first analysis of its performance. This was done in parallel with other experiments conducted at the INAF-Padova laboratory and at the Laboratoire d'Astrophysique de Marseille (LAM). In the first case, we realized a test-bench resembling the ELT characteristics in order to become familiar with the optical and geometrical properties of the ingot,[6,7] studying its response to low order aberrations

Send correspondence to EP. E-mail: elisa.portaluri@inaf.it, Telephone: +39 049 8293 447

Adaptive Optics Systems VII, edited by Laura Schreiber, Dirk Schmidt, Elise Vernet, Proc. of SPIE
Vol. 11448, 114483I · © 2020 SPIE · CCC code: 0277-786X/20/$21 · doi: 10.1117/12.2562190

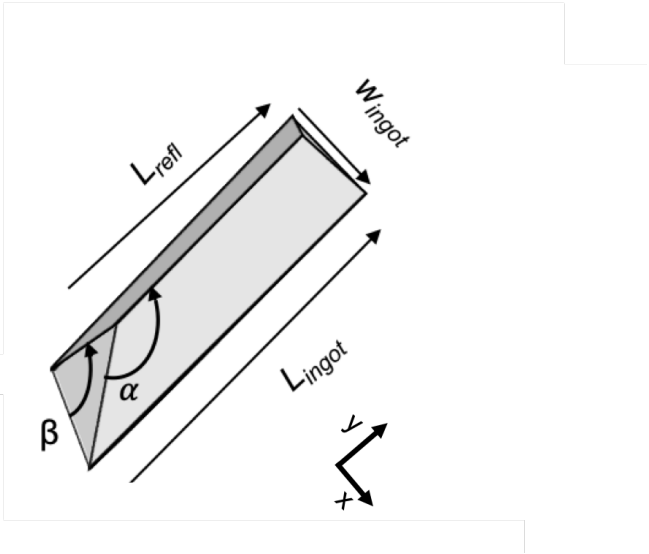

Figure 1. Schematic representation of the ingot solid shape and the parameters used to describe its geometry. The reference axes used to calculate the slopes are shown in the corner. Note that the simulation tool described in this work accepts the projection of ingot length on the FP, $L_{in,FP}$, instead of its total length L_{ingot}, as indicated in Table 1. L_{refl} is the minimum length of the reflective face.

and identify an alignment procedure. Moreover, at LAM we used the LOOPs bench emulating a 2D version of the ingot in a quasi-real AO system.[8]

In Section 2 we briefly discuss the general flux of the simulation tool, while in Section 3 we go into details of the tests made for the assessment of the tool itself, by varying input parameters and considering different conditions/configurations. Then, we describe in Section 4 an example of a closed loop, which we consider as a starting point to setup a proper set of simulations with statistics significance (Section 5).

2. SIMULATION TOOL CODE FLUX

The tool we developed is written in the Interactive Data Language (IDL) version 8.7. It is aimed at the estimation of the performance of the I-WFS, mounted to an user-defined telescope, under different conditions. It starts from a large set of parameters set by the user and simulates closed loop AO operations including wavefront sensing, reconstruction and correction, minimizing the rms wavefront error.[9,10] Now we consider a single LGS, however a proper MCAO approach with multiple LGS is planned.

The package includes about 100 different routines that can be called independently (computing different steps required by the overall simulation), in a object-oriented environment fashion, and it takes advantage of the IDL astronomy user's library.[11]

Here we report the main blocks containing the input parameters that can be used to customize the simulation. As an example, we report the values/assumption we adopted mimicking the ELT configuration. In particular:

- we used a frozen atmosphere (for the moment), equivalent to assuming an infinite computing power for the real time control loop. The turbulence follows a von Karman spectrum, and approximated by the 35-layers ESO profile,
- we assumed a constant flux profile of the Na layer,
- we adopted the telescope characteristics foreseen for the ELT and for the LGS Launcher Telescope (LLT),
- we selected a strategy for the LGS approximation (see the Section 3 for the details), and
- the size of the ingot has been adjusted according to the extension of the LGS image.

Table 1. Input Blocks of the simulator

Atmosphere inputs	C_n^2 profile	35 layers
	Seeing characteristics	$r_0 = 0.14$ m; $L_{0,max} = 25$ m; $l_{0,min} = 0.001$ m
	Spectrum type	von Karman
	Sodium layer mean altitude	88000 m
	Sodium layer thickness	15000 m
System inputs	Telescope Diameter	38.5 m
	LLT position (XY coords)	(-21.5, 0) m
	LGS position (XY coords)	(-21.5, 0) m
	Entrance pupil shape	ELT pupil mask
	λ_{WFS}	5.89×10^{-7} m
LGS inputs	Grid style	Gaussian 1D
	Na profile	fixes profile, 11 layers
	Na sampling	0.003 per meter
	XY size of LGS cigar	1.5", corresponding to 0.65 m @ 90km
	LGS sampling (XY plane)	500 points
Ingot WFS inputs	Ingot size	$L_{in,FP} = -0.010$ m, $W_{ingot} = 0.016$ m, $\alpha = 83.63°$, $\beta = 28°$
	Pupil sampling	n. actuators over diameter = 80
	Pupil geometry	ELT pupil mask rebinned at 38×38 px^2

3. FIRST TESTS AND ANALYSIS

A great effort has been devoted to choose the entire philosophy of the code, especially focusing on the appropriate approach to get reliable results. The general flux is analogous to the one used by other tools dedicated to wavefront sensing simulations, but it is different in some aspects because of the peculiar shape of the LGSs and of the geometrical characteristics of the I-WFS itself. A major trade-off was that of choosing between a Fourier transform approach and the ray tracing one, ending with an hybrid mode.[9] This selected approach is driven by two main considerations: the need for speed and the will of an opportune spatial resolution.

3.1 LGS approximation

The bottleneck in the efficiency of the code was especially the high number of points necessary to properly represent the LGS 3D shape. In fact, each point source needs to be optically and geometrically propagated in the whole system, crossing a given aperture and ending on a certain face of the ingot prism. As described in Viotto et al. (2019), we accounted 3 different representations of the LGS cigar:

- 3D sampling: a 3D grid, in which the vertical profile matches the Na layer density spatial variations and the radial one follows a Gaussian law mimicking the intensity of atoms excitement.
- 2D sampling: the sampling only occurs on the vertical plane, inside the LGS, which focuses on the Ingot prism main plane.
- 1D sampling: the LGS is approximated as a number of layers with a cylindrical shape. In this case the sampling is related to the LGS axis, which focuses on the ingot prism roof edge and each "slice of LGS" has a Gaussian profile and is convolved with a mask representing the ingot prism main plane, having a different shape for each sub-aperture.

The three approaches are listed in order from the most expensive to the simpler one, in terms of number of points to be considered and, therefore, in terms of computational time/speed. We tested all of them, ending with comparable data and verifying the consistency of the results, in a low-resolution configuration, obtained

re-scaling the ELT pupil mask from 380×380 px^2, to 38×38 px^2 and, thus, reducing the number of sub-apertures to be considered.

Full resolution simulations require more time and, for this reason, we used the faster 1D approach. A drawback of this approach is that it requires to store, for every sub-aperture, the image produced by a slice of the LGS, leading to demanding requirements in terms of memory. The workstation we used was totally dedicated to the simulations, and has these characteristics: a Due Intel Xeon Gold Processor with 3.4 GHz (3.7 GHz Turbo) with 6 cores and a 128 GB RAM (8 x 16 GB) at 2.666 MHz.

A first attempt to reduce the memory requirements has been to parametrize the shape of the spot produced by every sub-aperture, in order to find a correlation between the input parameters used to configure the LGS on the atmosphere, and the spot itself, as a function of the corresponding sub-aperture. Doing this, it is not necessary anymore to store a high-resolution image of the spot, because the image can be calculated from the input parameters. The shape of the spot depends on the profile chosen for the LGS sampling: if the source is approximated as an uniform circle, then we expect that the ingot produces an ellipse, while the spot will have a 2D Gaussian elliptical shape, if the LGS slice is approximated to a Gaussian profile (i.e., to resemble the intensity of atoms excitement). An optimal prediction of the shape of such a ellipse could help us in saving computational memory (and time), avoiding the propagation of each point through the system. We opted for the last option, a configuration closest to the reality: the spot is parametrized by a 2D Gaussian approximation, whose dispersion varies significantly in the X direction as the distance from the launcher increases (Figure 2).

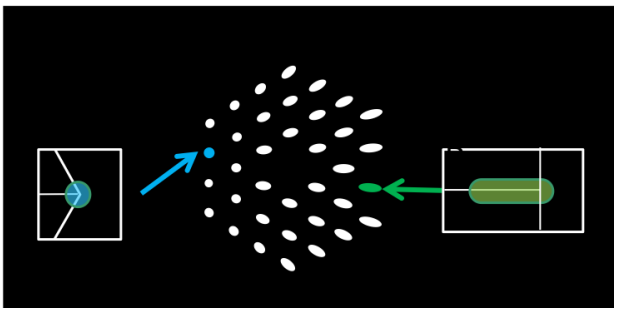

Figure 2. Schematic representation of the spot elongations due to the distance of the LLT firing the LGS to the WFS. This effect is due to the geometry of the LGS itself (finite distance and 3D shape). On the side we reported as the ingot is seen from the corresponding sub-apertures.

The LLT is placed on 21.5 m on the left of the telescope system (as seen from the top), therefore, as expected, sub-apertures close to the launcher "produce" spots that are less elongated with respect to more distant ones.

Figure 3 shows an example of a sub-aperture analyzed with this method, using a 2D Gaussian function, truncated at 1 sigma. Fitting all the sub-apertures, we obtained a map of the Gaussian parameters and we looked at them finding, eventually, a relation (Figure 4). The center positions are almost constant, varying only in very left part of the pupil. To investigate the robustness of the fit, we plotted the same parameters also in 1 dimension and performed the correlations between the observed and fitted image (Figure 5). When the spots are more elongated, the fits failed in recovering correctly the parameters.

The difficulties found in fitting the very elongated ellipses made us to consider different approaches, because of the importance of those spots in the consideration of the whole performance of the sensor, as it is conceived to cope as much as possible the geometry of the LGSs.

The solution was given simply by algebric considerations and reducing the complexity of the system. First, using the 1D sampling approach, we can consider the LGS composed by a number of disks, slicing the whole cigar, instead of considering the cylinders. Each disk can be approximated by a Gaussian profile. A circular slice of the LGS is imaged into an ellipse by the ingot. In order to reconstruct the parameters of such an ellipse (center coordinates, orientation and semi-axis length) it is sufficient to find the projection 5 points positioned on the circumference of the circle. Then, we can reconstruct the 2D shape of the spot assigning "a posteriori" the appropriate 2D Gaussian profile. The equations used in this approach are described in the Figure 6.

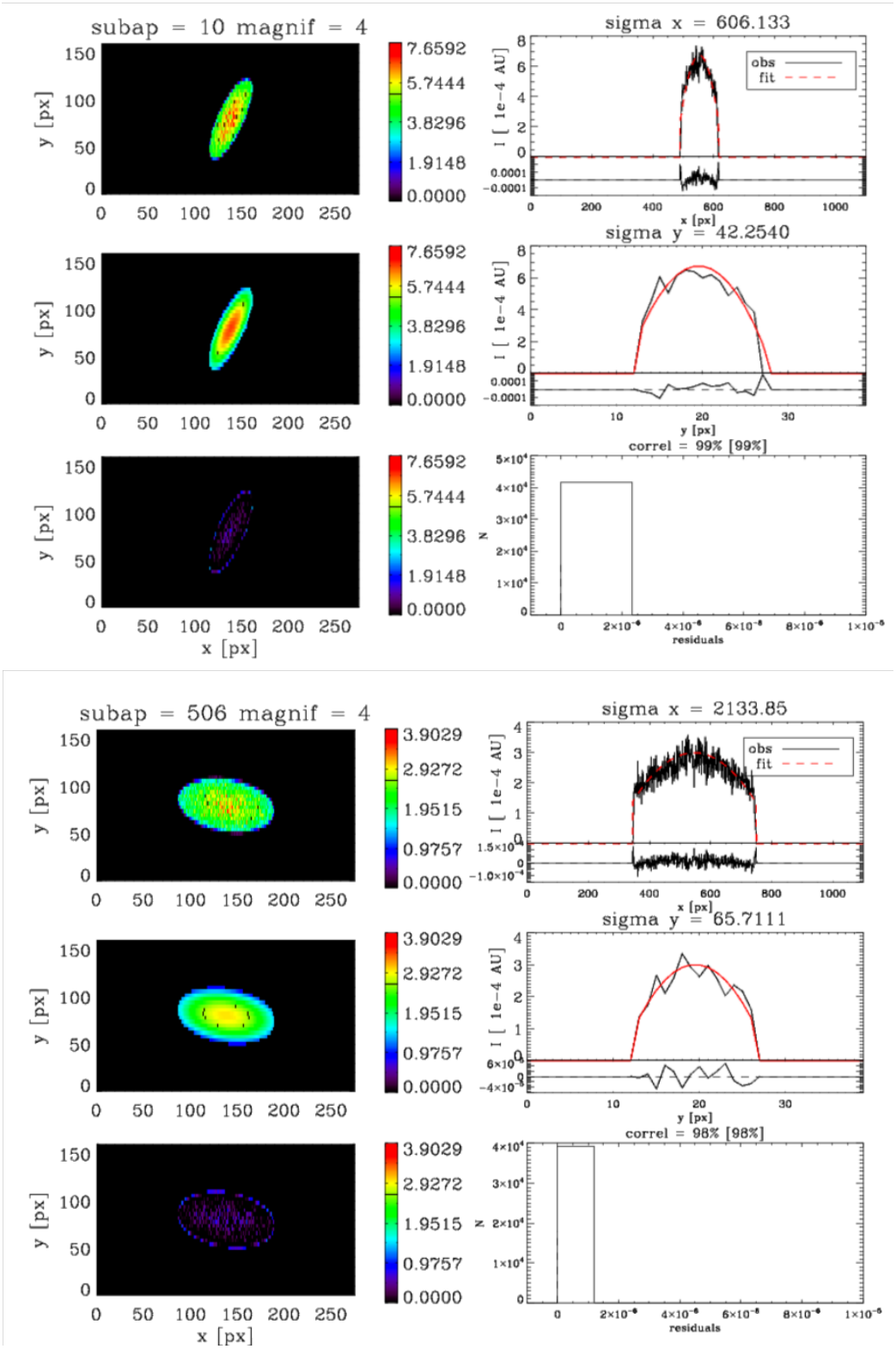

Figure 3. Example of the fit done on two sub-apertures. Left panel: image (top) and 2D Gaussian fit (center) of the disk generated by the propagation of a single slice the LGS (1D approach, see the text for more details). The bottom panel shows the residuals, measured as the difference between the two images. The colorbar scale is logarithmic. Right panel: 1D profile of the disk (in black) and Gaussian fit (in red), considering the central slit with respect to the X (top) and Y (center) axes. The bottom plot shows the histogram of the residuals, which are about a few %.

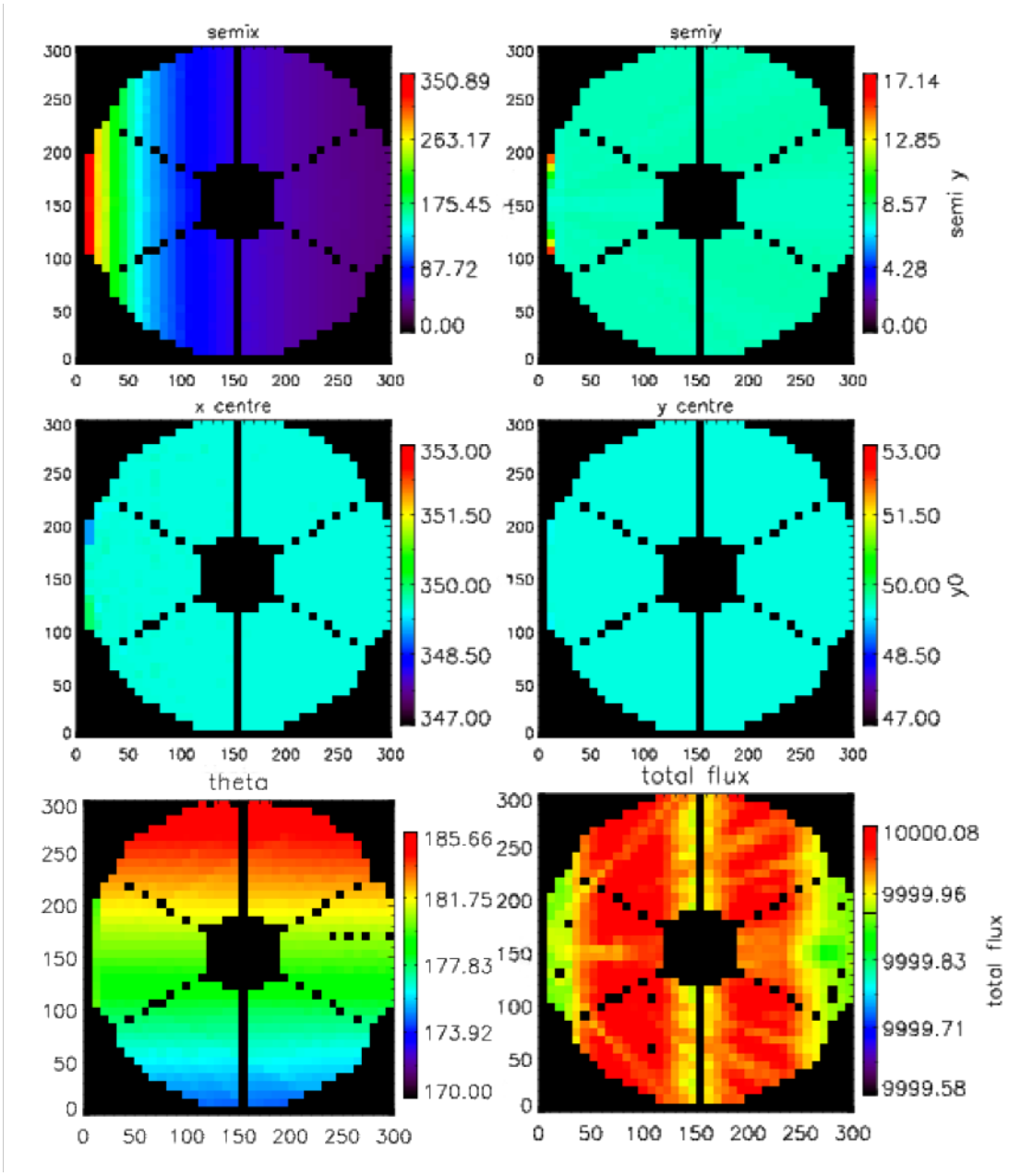

Figure 4. 2-dimensional maps of the Gaussian parameters found during the fit of the disks produced on the FP from the propagation of the LGS through the system. The semi-major axes (top), the positions of the center in both the dimensions (center), and the inclination and total flux (bottom) are shown.

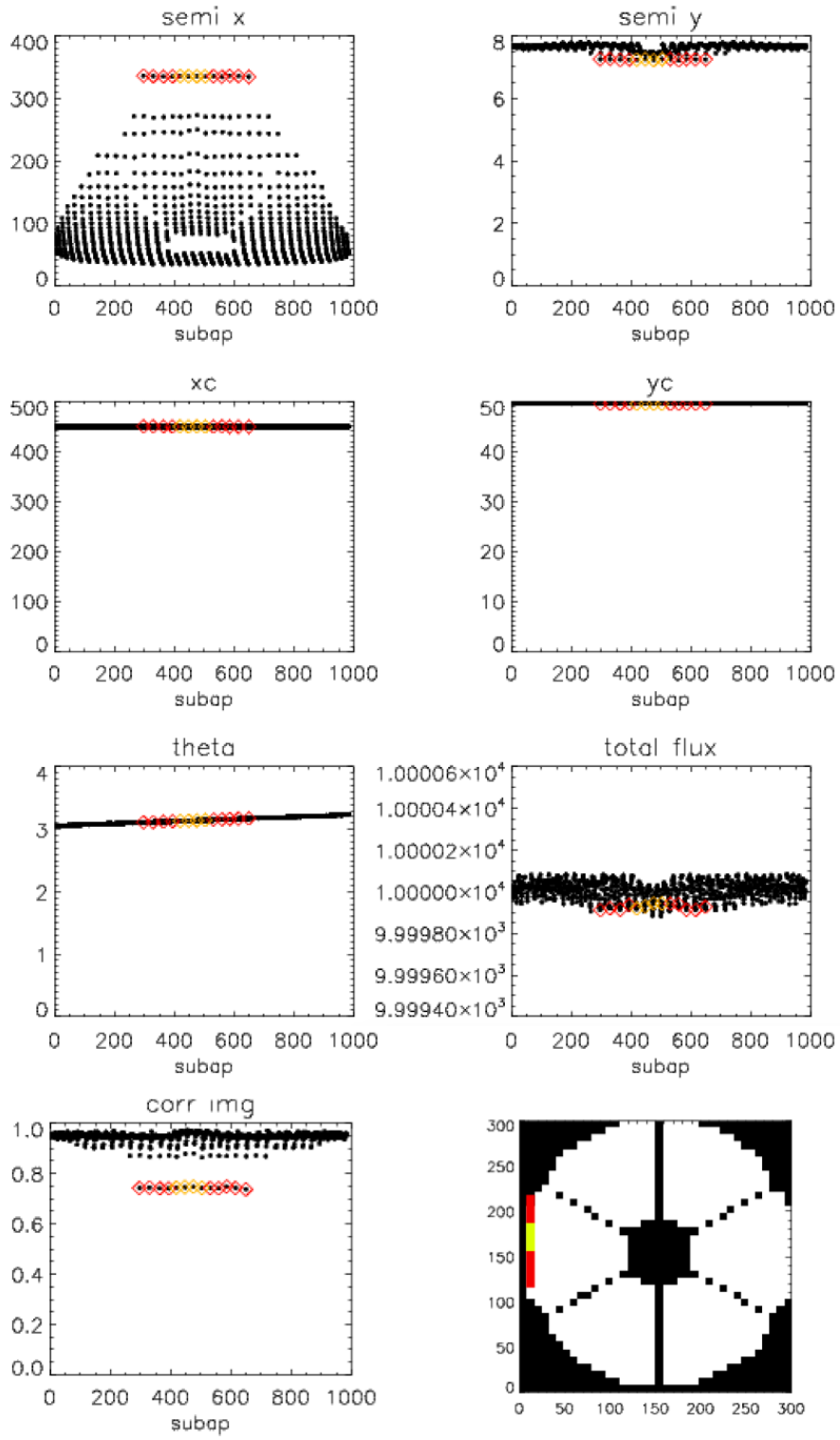

Figure 5. Same as in Figure 4, but in 1 dimension. The last line of the plot shows the correlations between the two images: the real and the fitted ones. The colored squares mark the sub-apertures where the correlation is low and are shown in the maps of the ELT pupil mask. Looking by eye we noticed that the failure of the fit is due to the bad recovering of the semi-major axis (yellow squares) and both axes (red squares). This is due to the very high ellipticity of the disks far to the LLT (left sub-apertures).

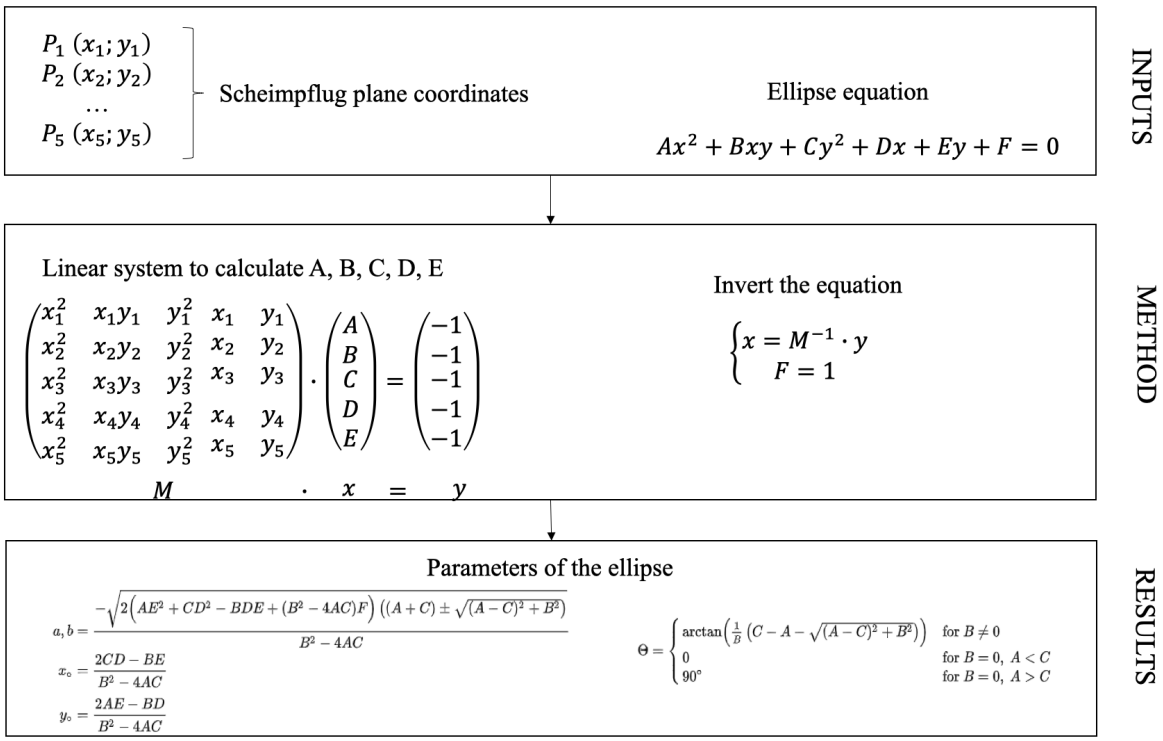

Figure 6. Block diagram of the procedure used to reconstruct the spot elongation pattern, considering a single slice of LGS in the 1d sampling approximation. 5 points located on the contour of the slice are propagated through the system and reach the Scheimpflug plane. There, the spot is reconstructed for each sub-aperture, using the parameters of the ellipses calculated as in the equation above. Then, a 2D Gaussian profile is assigned to mimic the light intensity distribution.

3.2 Slope measurement

The signal of the ingot is computed, from the re-imaged pupils, in a 3-quad-like style, using the light on the pupils produced by the 2 lateral faces to compute the wavefront derivative along both the axis, and the light in all the 3 faces only to compute the derivative signal in the direction parallel to the spot elongation (Y).

We considered several options to obtain the signals: one is using the pupil flux directly, ending with 3 signals. For the other two methods we measured quantities proportional to the wavefront first derivatives, whose equations are reported in Table 2, assuming A as the transmitted pupil, while B and C are the reflective ones. We used as a reference, the signals obtained with a flat wavefront, i.e. the static of the system. In fact, even in absence of aberrations, all the rays spread on the prism faces with a non uniform distribution, because of the geometry of the system.

Table 2. Different equations measuring the slopes.

Option	S_x	S_y
Signal_1	$S_x = \left(\frac{B-C}{B+C}\right) - \left(\frac{B-C}{B+C}\right)_{stat}$	$S_y = \left(\frac{B+C-A}{A+B+C}\right) - \left(\frac{B+C-A}{A+B+C}\right)_{stat}$
Signal_2	$S_x = \left(\frac{B-C}{A+B+C}\right) - \left(\frac{B-C}{A+B+C}\right)_{stat}$	$S_y = \left(\frac{A}{A+B+C}\right) - \left(\frac{A}{A+B+C}\right)_{stat}$

Figure 7 shows the slopes obtained calculating S_x and S_y in the three cases considered. The static is already subtracted.

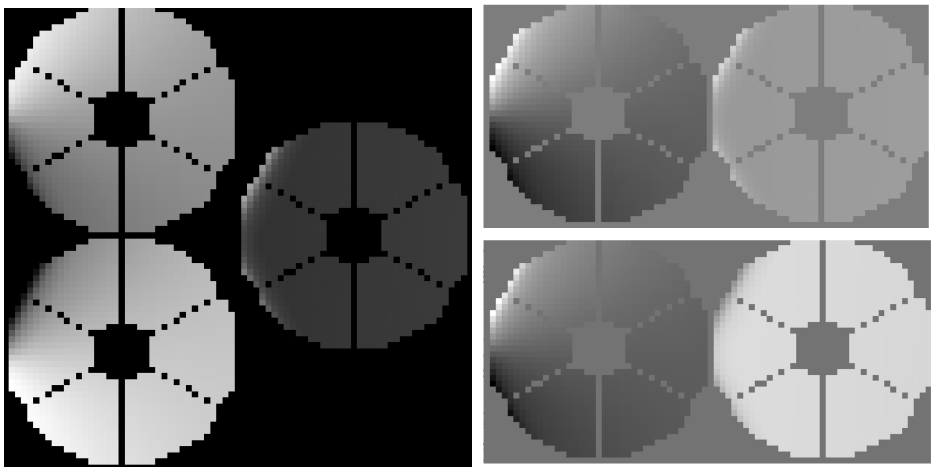

Figure 7. 2D slopes calculated with the three different methods: a) directly from the 3 pupils (left panel), b) from the equations "Signal_1" (top-right panel) and, c) "Signal_2" (bottom-right panel) reported in Table 2.

4. CLOSING A LOOP

We ran some simulations to estimate the preliminary I-WFS performance, in low-resolution mode.

Figure 8 shows an example of a reconstruction in a close loop where an input wavefront built using a Zernike basis is recovered. In this case we used the equation of Signal_1 reported in Table 2, and the inputs listed in Table 1. The input wavefront was generated using the Noll coefficients for 100 Zernike modes, as shown in Figure 9. The residuals are 3 orders of magnitude less than the inputs, therefore we can conclude that we were able to close the loop and perform a good reconstruction of the wavefront, even in this preliminary stage.

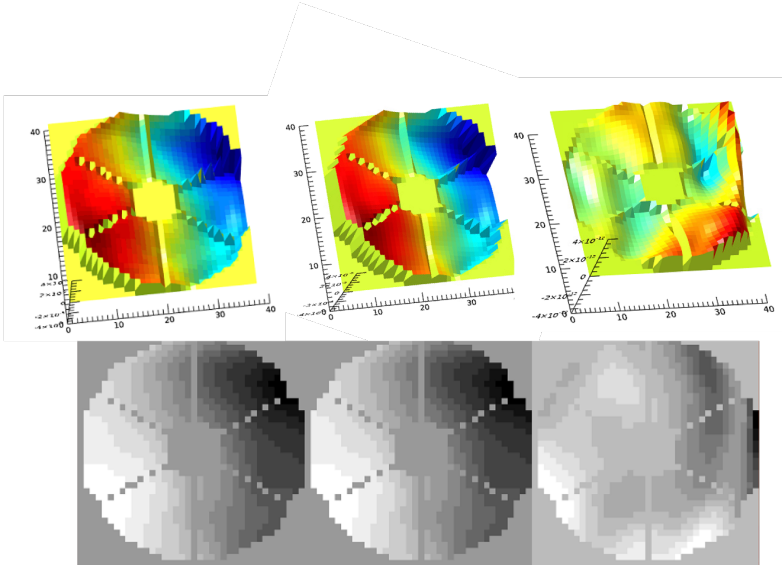

Figure 8. Example of a reconstruction made using input parameters listed in Table 1. Top: 3D shape of the input (left) and reconstructed (center) wavefront, and the corresponding residuals (right). The input was generated using the Noll coefficients (C_{in}) for 100 Zernike modes. Bottom: as the top, but in 2 dimensions.

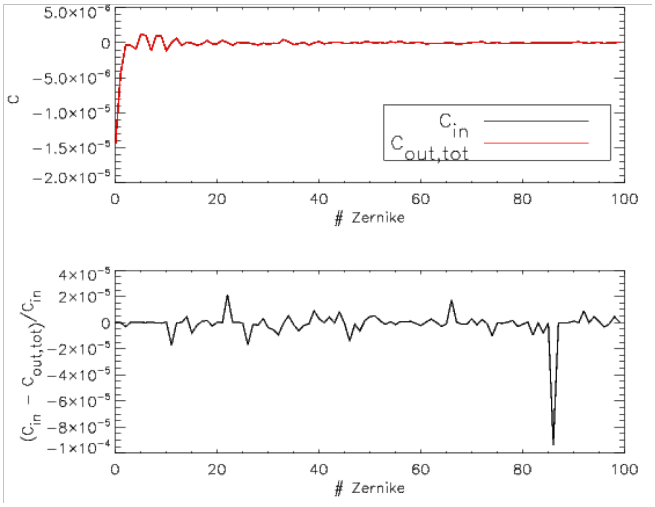

Figure 9. Example of a reconstruction. 100 Noll coefficients (C_{in}) used as input (black line) and recovered (C_{out}) after the reconstruction (red line). The bottom plot represents the residuals.

5. DISCUSSION AND FUTURE DEVELOPMENT

We have set up a simulation tool to evaluate the ingot performance.

Basically, assuming a certain system geometry and LGS asterism, accounting for the cone effect and for a given atmosphere, we can retrieve the incoming wavefront, which is then translated into the focal plane, through the ingot, to the pupil plane, where the 3 pupils are re-imaged and then used to compute signals. The simulator is fed by a variety of input parameters and flag options: some of them are describing the telescope system, others are for the atmosphere and for the LGS approximation. The interaction matrix is computed using a Zernike modal basis, and the relative reconstructor is calculated and then used to retrieve the output wavefront from signals, measured with different options. We performed first loop in low-resolution mode and we were able to properly close them and obtain very good performance.

The need to speed-up the code and the computational memory problems has been solved, therefore we are ready to improve the simulations changing the input parameters as resolution, sampling, number of modes and dynamical disturbance to have a full description of the performance, which at the end we plan to compare with those obtained using the a SH-WFS.

This work is going in parallel with first experiments on the laboratory[7] and also with simulations in the Fourier environment,[8] therefore we will have a complete view to evaluate the positive impact of such a sensor on an AO system, going towards the possibility to test it on sky.

ACKNOWLEDGMENTS

This work is supported by the INAF Progetto Premiale "Ottica Adattiva Made in Italy per i grandi telescopi del futuro".

REFERENCES

[1] Ragazzoni, R., Portaluri, E., Viotto, V., Dima, M., Bergomi, M., Biondi, F., Farinato, J., Carolo, E., Chinellato, S., Greggio, D., Gullieuszik, M., Magrin, D., Marafatto, L., and Vassallo, D., "Ingot Laser Guide Stars Wavefront Sensing," *AO4ELT5 Proceedings* (Aug. 2017).

[2] Ragazzoni, R., Greggio, D., Viotto, V., Di Filippo, S., Dima, M., Farinato, J., Bergomi, M., Portaluri, E., Magrin, D., Marafatto, L., Biondi, F., Carolo, E., Chinellato, S., Umbriaco, G., and Vassallo, D., "Extending the pyramid WFS to LGSs: the INGOT WFS," in [*Adaptive Optics Systems VI*], Close, L. M., Schreiber, L., and Schmidt, D., eds., *Society of Photo-Optical Instrumentation Engineers (SPIE) Conference Series* **10703**, 107033Y (July 2018).

[3] Ragazzoni, R., Viotto, V., Portaluri, E., Bergomi, M., Greggio, D., Di Filippo, S., Radhakrishnan, K., Umbriaco, G., Dima, M., Magrin, D., Farinato, J., Marafatto, L., Arcidiacono, C., and Biondi, F., "Pupil plane wavefront sensing for extended and 3d sources," in [*AO4ELT6*], (2019).

[4] Gilmozzi, R. and Spyromilio, J., "The European Extremely Large Telescope (E-ELT)," *The Messenger* **127** (Mar. 2007).

[5] Johns, M., "The Giant Magellan Telescope (GMT)," in [*Extremely Large Telescopes: Which Wavelengths? Retirement Symposium for Arne Ardeberg*], Proc. SPIE **6986**, 698603 (Apr. 2008).

[6] Di Filippo, S., Greggio, D., Bergomi, M., Radhakrishnan, K., Portaluri, E., Viotto, V., Arcidiacono, C., Magrin, D., Marafatto, L., Dima, M., Ragazzoni, R., Janin-Portirond, P., Schatz, L., Neichel, B., Fauvarque, O., and Fusco, T., "Ingot wavefront sensor: from the optical design to a preliminary laboratory test," in [*AO4ELT6*], (2019).

[7] Santhakumari, K. K. R., Greggio, D., Bergomi, M., Di Filippo, S., Viotto, V., Portaluri, E., Arcidiacono, C., Dima, M., Luigi, L., Marafatto, L., Furierie, T., Bonorae, S., and Ragazzoni, R., "Aligning and Testing the Ingot Wavefront Sensor in the Lab," in [*This Conference*], *Society of Photo-Optical Instrumentation Engineers (SPIE) Conference Series* (Dec. 2020).

[8] Arcidiacono, C., Di Filippo, S., Santhakumari, K. K. R., Greggio, D., Viotto, V., Portaluri, E., Ragazzoni, R., Bergomi, M., Marafatto, L., Dima, M., Magrin, D., Farinato, J., Janin-Potiron, P., Fusco, T., Neichel, B., Fauvarque, O., and Schatz, L., "Ingot Wavefront Sensor: from the Fourier End2End numerical simulation to the LOOPS test bench," in [*This Conference*], *Society of Photo-Optical Instrumentation Engineers (SPIE) Conference Series* (Dec. 2020).

[9] Viotto, V., Portaluri, E., Arcidiacono, C., Ragazzoni, R., Bergomi, M., Di Filippo, S., Dima, M., Farinato, J., Greggio, D., Magrin, D., and Marafatto, L., "Dealing with the cigar: preliminary performance estimation of an INGOT WFS," in [*Adaptive Optics Systems VI*], Close, L. M., Schreiber, L., and Schmidt, D., eds., *Society of Photo-Optical Instrumentation Engineers (SPIE) Conference Series* **10703**, 107030V (July 2018).

[10] Portaluri, E., Viotto, V., Ragazzoni, R., Arcidiacono, C., Bergomi, M., Greggio, D., Radhakrishnan, K., Di Filippo, S., Marafatto, L., Dima, M., Biondi, F., Farinato, J., and Magrin, D., "Ingot wfs for lgss: First results from simulations," in [*AO4ELT6*], (2019).

[11] Landsman, W. B., "The IDL Astronomy User's Library," in [*Astronomical Data Analysis Software and Systems II*], Hanisch, R. J., Brissenden, R. J. V., and Barnes, J., eds., *Astronomical Society of the Pacific Conference Series* **52**, 246 (Jan. 1993).